Letter to the Editor

Cartilaginous endplate coverage of developmental Schmorl's node and the relevance of this in Schmorl's node etiology-based classification

Yì Xiáng J. Wáng^

Department of Imaging and Interventional Radiology, Faculty of Medicine, The Chinese University of Hong Kong, Shatin, Hong Kong SAR, China

Correspondence to: Yì Xiáng J. Wáng, MMed, PhD. Department of Imaging and Interventional Radiology, The Chinese University of Hong Kong, 30-32 Ngan Shing Street, Shatin, New Territories, Hong Kong SAR, China. Email: yixiang_wang@cuhk.edu.hk.

Submitted Feb 20, 2024. Accepted for publication Apr 22, 2024. Published online May 09, 2024.
doi: 10.21037/qims-24-335
View this article at: https://dx.doi.org/10.21037/qims-24-335

We have recently classified Schmorl's node (SN) into two categories: SN of primarily developmental cause (SNd) and SN of primarily acquired cause (SNa), though it is highly likely that in many cases the cause could be muti-factorial (1). This classification has been taken up by colleagues (2). We noted that small SNd may not have clinical relevance, and they may be well covered with endplate (1). In this letter, we further suggest that, according to the cartilaginous endplate coverage, SN can be classified into SN with intact cartilaginous endplate coverage and SN without intact cartilaginous endplate coverage (*Figure 1*). We postulate that SNd is with cartilaginous endplate coverage, and SNa is without intact cartilaginous endplate coverage. Nowadays, ultra-short time-to-echo (UTE) MRI technique can clearly demonstrate cartilaginous endplate (3-8). We recently systematically searched and checked the published spine UTE-MR image with SN, and it appears that the available evidence supports this hypothesis (9-15) (*Figures 2-6*). The intrinsic lack of blood vessels, nerves, and lymphatic vessels within cartilage tissue severely limits its self-regenerative capacity after injury. The same as articular cartilage, once damaged, cartilaginous endplate is limited in its ability to repair itself. Based on the cartilaginous endplate coverage of SN and for the convenience of recording radiological observations, we classify SN into four types (*Figure 7*):

- *Type-1A*: this is the most common and typical type of SNd (1,16) (*Figures 2,3,8-10*). SNd of type-1A has a fixed location, i.e., posterior part of the endplate. At any time point of imaging, SN type-1A should not be complicated with observable signs of SNa, particularly edema on T2-weighted MRI or increased activity on radioisotope imaging, otherwise they are classified into type-3.
- *Type-1B*: these are SNd excluding those of type-1A, and associated with less common causes such as those shown in *Figures 11-16* (17-21). One feature of SN type-1B is that the location is not typically at the posterior part of the endplate as with type-1A. SN type-1B is commonly seen with Scheuermann's disease and mucopolysaccharidosis type-1. Another reported location of SN type-1B is the anterior upper corner of the vertebral body (17) (*Figures 11,12*).
- *Type-2*: this is the most common type of SNa (*Figures 4-6,17-21*). This type of SN has recognisable features of SNa or with typical clinical history, but without the features of SNd. Features of SNa include relatively large in size, incomplete bony sclerotic border, and hazy cloudy increased density surrounding the NS. Edema on T2-weighted MRI or increased activity on radioisotope imaging can be

^ ORCID: 0000-0001-5697-0717.

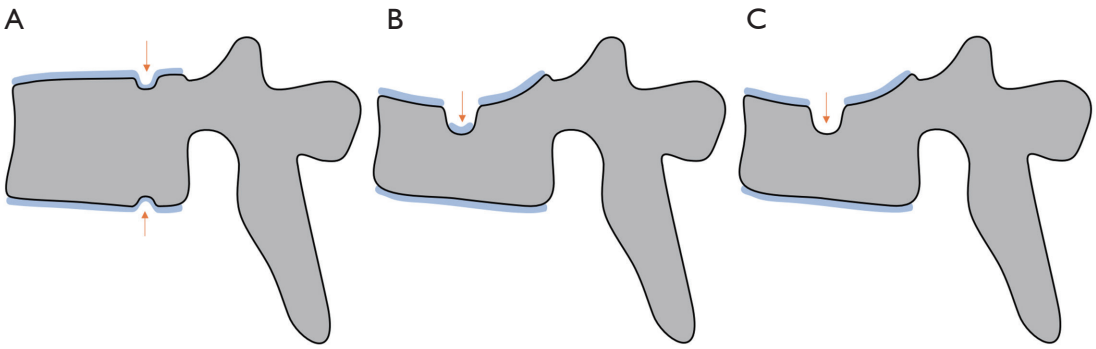

Figure 1 An illustration of cartilaginous endplate coverage of SN. (A) Two SNd with continuous cartilaginous endplate coverage (type-1A), however the covered cartilaginous endplate may be thinner and less regular (arrow). (B) A SNa with only partial remanent cartilaginous endplate (type-2, arrow). (C) A SNa without cartilaginous endplate coverage (type-2, arrow). It is highly possible that low BMD and osteoporosis is the most common etiology for SNa among elder populations, thus osteoporotic-like vertebral fracture can be a commonly associated imaging finding for these SNa. SN, Schmorl's node; SNd, Schmorl's node of developmental cause; SNa, Schmorl's node of acquired cause; BMD, bone mineral density.

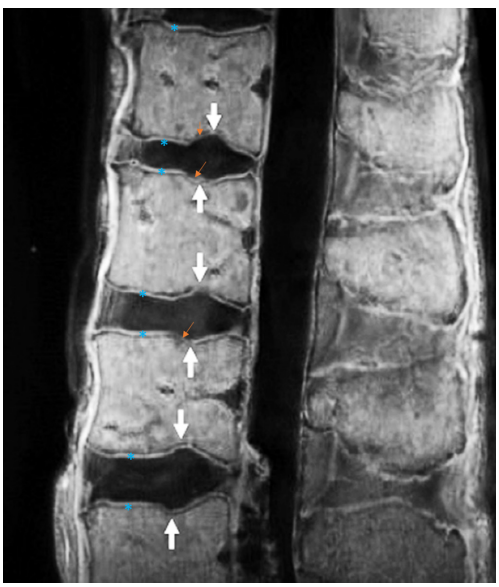

Figure 2 UTE *ex vivo* MR image shows multiple typical SN type-1A. The locations are very typical for this type of SN. The cartilaginous endplate (blue asterisks) covering the SNs appears to be continuous (arrows), though these parts appear to be thinner or less regular (brown small arrows) and may appear discontinuous artificially when the spatial resolution is insufficient. Reused with permission from Siriwanarangsun *et al.* (8). UTE, ultrashort time-to-echo; MR, magnetic resonance; SN, Schmorl's node.

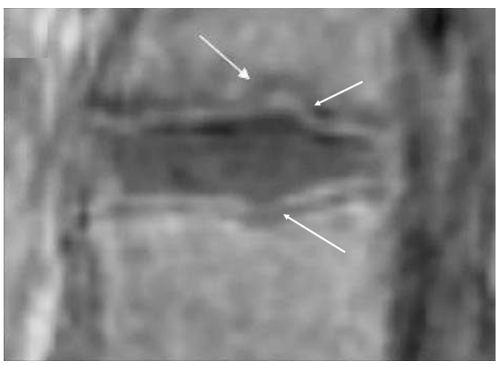

Figure 3 UTE image shows two typical SN type-1A. The locations are very typical for this type of SN, involving the lower endplate of an upper vertebra and the upper endplate of a lower vertebra, and at the junction of anterior 2/3 and posterior 1/3 of the endplates. The cartilaginous endplate covering the two SNs appears to be continuous (arrows). Reused with permission from Ji *et al.* (15). UTE, ultrashort time-to-echo; SN, Schmorl's node.

seen at the acute phase, though these changes will fade away after the acute phase. This type of SN is not in the typical location of type-1A (otherwise, they are classified into type-3).

- *Type-3*: SN of mixed and developmental acquired

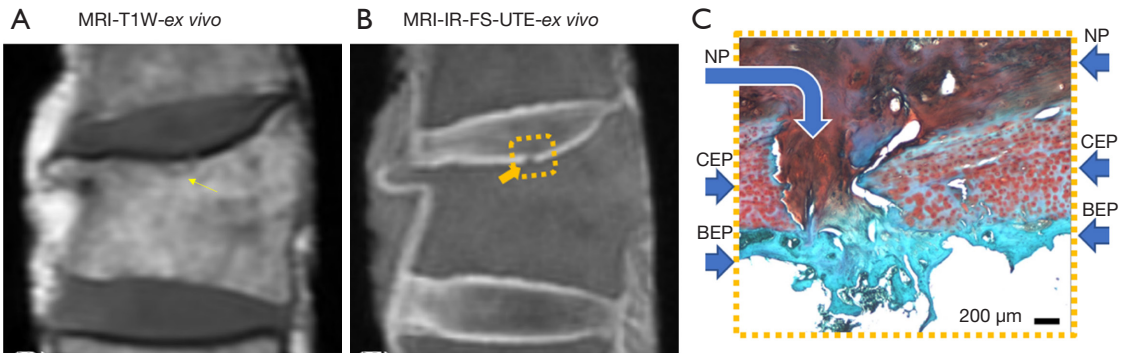

Figure 4 A small SN without cartilaginous endplate coverage (type-2). (A) T1w *ex vivo* MR image of a vertebra with compressive fracture and a small SN (arrow). (B) IR-FS-UTE *ex vivo* MR image shows cartilaginous endplate of high signal (square). The defect of the SN is shown (arrow). (C) Histology image: curved arrow denotes disruption of the CEP, straight arrow denotes NP, CEP, and BEP. Reused with permission from Lombardi *et al.* (9). MRI, magnetic resonance imaging; T1w, T1-weighted; IR, inversion-recovery-prepared; FS, fat-saturated; UTE, ultrashort time-to-echo; NP, nucleus pulposus; CEP, cartilaginous endplate plate; BEP, bony endplate plate; SN, Schmorl's node; MR, magnetic resonance.

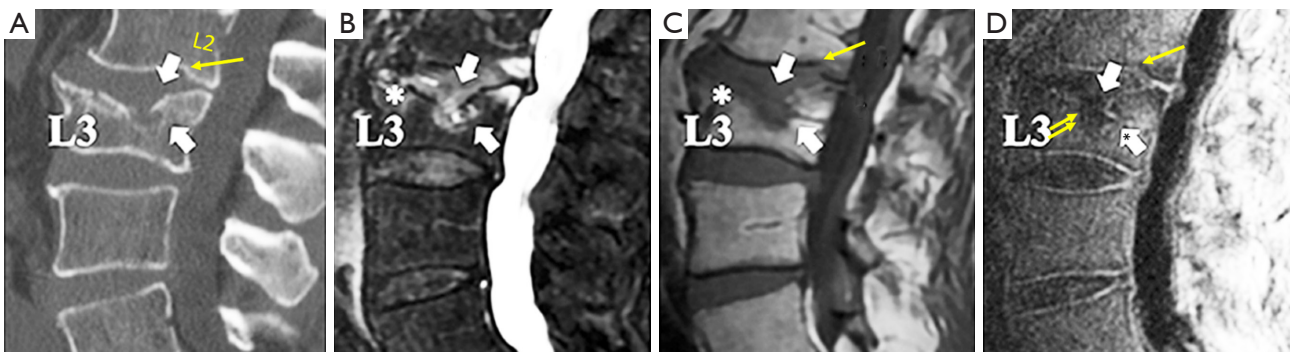

Figure 5 Vertebral L3 osteoporotic-like fracture and upper endplate SN type-2, as well as L2 lower endplate SN type-1A, with sagittal reconstructed *in vivo* CT image (A) and sagittal T2-weighted and T1-weighted images (B,C) as well as sagittal IR-FS-UTE images (D). T2 weighted image shows areas of bone marrow edema, especially in L3 (white asterisk). The cartilaginous endplate plate is seen on the IR-FS-UTE imaging (D), and it is discontinuous in the areas of fracture SNa entry (arrowheads and arrows in D). However, a residual amount of cartilaginous endplate can be appreciated (white arrow with a black asterisk). Reused with permission from Lombardi *et al.* (9). SN, Schmorl's node; CT, computed tomography; IR, inversion-recovery-prepared; FS, fat-saturated; UTE, ultrashort time-to-echo; SNa, Schmorl's node of acquired cause.

causes (23,24) (*Figures 21-23*). This type of SN should have features of SNa which include incomplete bony sclerotic border and hazy cloud surrounding the NS, but in the meantime with features suggesting SNd nature, particularly the typical location of type-1A.

- *Type-4*: SN with uncertainty of acquired cause or developmental cause (*Figure 24*). In theory, there should be only SNa, SNd, or a SN of mixed developmental and acquire causes, but sometimes, such a determination of etiology may be difficult based on available imaging. These SNs are grouped into type-4 for practical recording.

Aside from etiology, subclassifications of type-2, type-3, and some type-4 may have the same clinical relevance. Differential clinical relevance will be more related to their pathogenesis causes such as being a trauma or osteoporosis, their size, and the severity of reactive inflammation, etc. The main relevance for type-4 is that it may actually belong to SNa in some cases. Considering the pathogenesis of SN

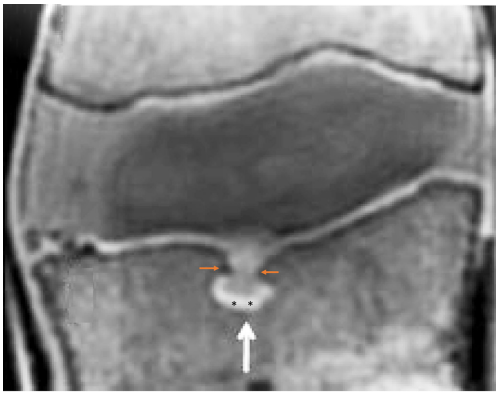

Figure 6 UTE MR image of a SN type-2 (white arrow). The cartilaginous endplate shows bright signal on the image, which is disrupted at the entry of SNa (brown arrows) and partially remains at the bottom of the SN (black asterisks). Note that the location of this SN is more anterior to the typical location of SN type-1A. Abruption and depression of adjacent bony endplate are also noted (brown arrows). Reused with permission from Lotz *et al.* (12). UTE, ultrashort time-to-echo; MR, magnetic resonance; SN, Schmorl's node; SNa, Schmorl's node of acquired cause.

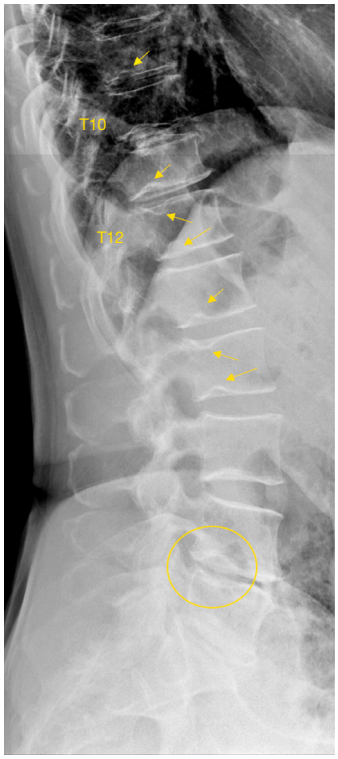

Figure 8 Radiograph shows multiple SN type-1A (arrows). The locations are very typical for this type of SN. T10/T11 disc space have calcified disc. L4 lower endplate shows 'cupid bow' (oval). SN, Schmorl's node.

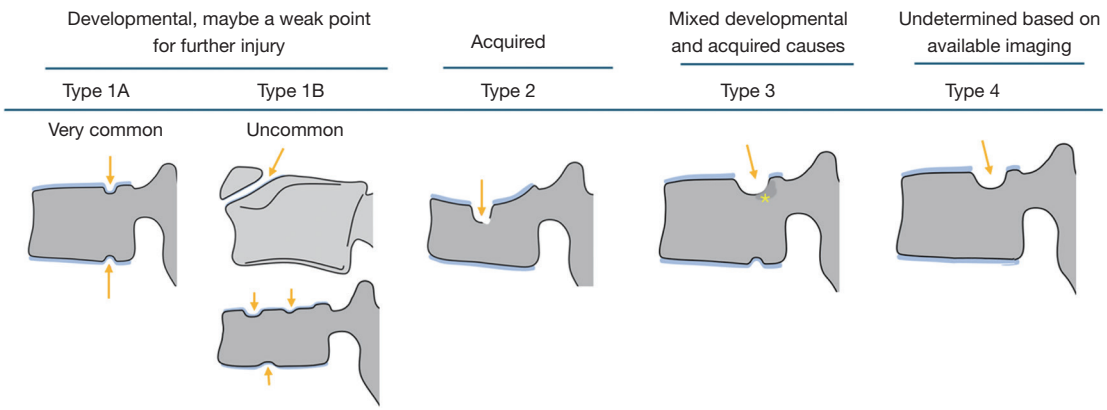

Figure 7 An illustration of four types of SN (arrows) classifications. Type-1A: SNd with continuous cartilaginous endplate coverage at the typical posterior part of the endplate and can involve both superior and inferior endplates. Type-1B: two types of less common SNd, with the lower example commonly seen in Scheuermann's disease. Type-2: an SNa without cartilaginous endplate coverage and the sclerotic border of the SN may be discontinuous. Among older population, it is likely that low BMD/osteoporosis is the most common etiology of SN type-2, and compressive deformity of the involved vertebra is commonly seen. Type-3: this SN is at the typical location of type-1A, but also with SNa signs such as larger in size and with hazy cloud surrounding (asterisk). Type-4: this SN is at the typical location of type 1A, with possible additional signs suggesting SNa such as a larger than expected size. SN, Schmorl's node; SNd, Schmorl's node of developmental cause; SNa, Schmorl's node of acquired cause; BMD, bone mineral density.

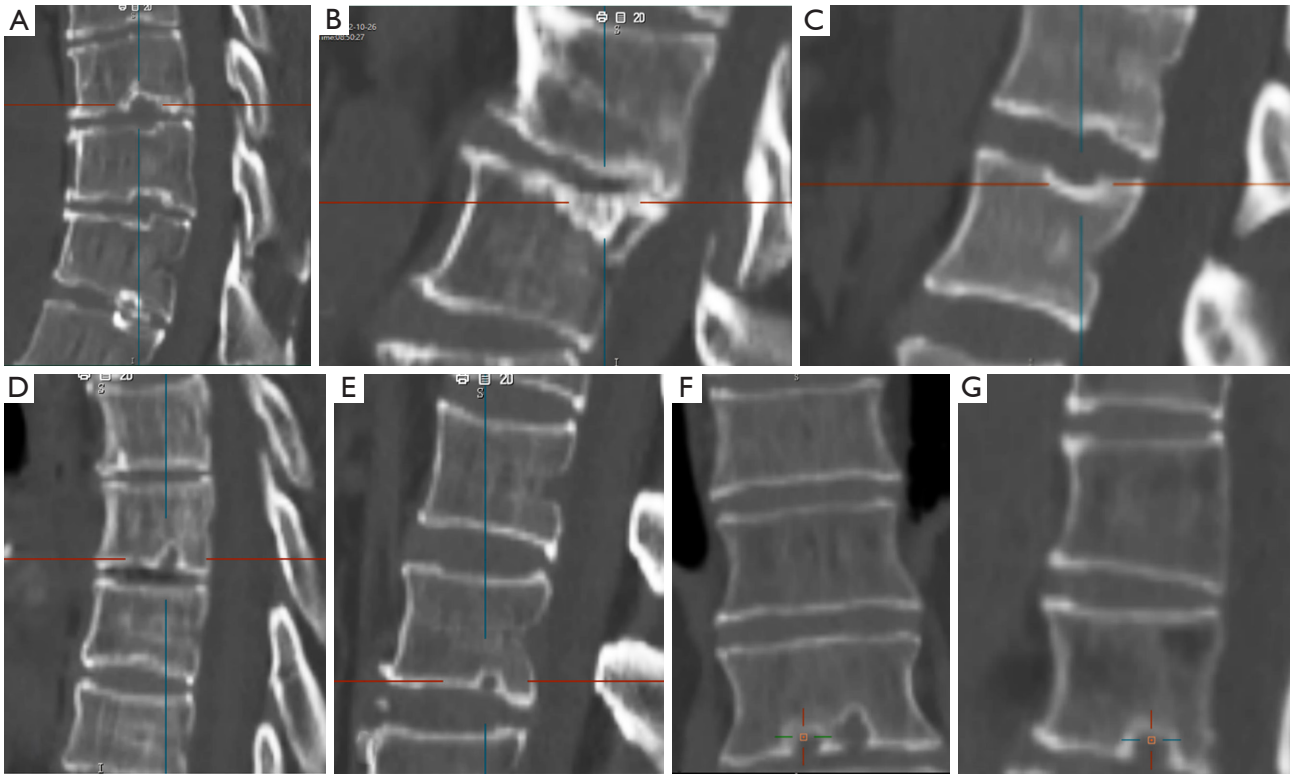

Figure 9 Sagittal CT reconstruction (A-G) shows SNd type-1A. Overall, these SNd have a clear and continuous sclerotic bony border, without apparent surrounding increased cloudy density that would reflect reactive bony regeneration. The location is very typical for this type of SNd, and at the junction of anterior 2/3 and posterior 1/3 of the endplates. Note that, in (C) the posterior portion of the superior endplate and in (G) the deep portion of the inferior endplate appear to be thick, but these are not considered as surrounding cloudy density. (F) and (G) are the same case. (F) with coronal view shows two SNd. CT, computed tomography; SNd, Schmorl's node of developmental cause.

formation can be multifactorial, for some SNs, a definite separation of SNd and SNa may not always be possible. We expect SNd is not due to a traumatic etiology occurring in the skeletally immature individual. SN due to a traumatic etiology occurring in the skeletally immature individual is also classified as SNa. SN classification may depend on imaging methods. It is possible that, while radiograph cannot determine its cause, high-resolution CT or UTE MRI may offer more precise classification.

The existence of SN type-3 suggests a weak point for the common location of type-1A. Walters *et al.* (25) describe a case of a female 14-year-old gymnast who developed an acute SN with edema MRI appearance, at L4 upper posterior endplates (i.e., typical location of SN Typical T1A). Conservative treatment led to the resolution of the symptoms of bone edema. Similar cases have been reported by Seymour *et al.* (24).

As we have described earlier (1), SN type-1A is characterized by that they more likely involve multiple adjacent vertebrae, more likely to be small or modest in size, and likely to have relatively consistent location. SNd tend to have a more solid border on radiograph due to their longstanding and sometimes static nature (*Figures 8-10*). According to its initial definition, SN corresponds histologically to nucleus pulposus herniation into the vertebral spongy bone with thickened trabeculae around the formed node. Resnick and Niwayama (20) noted that, *superior and inferior prolapse of disk material results in abnormalities at the discovertebral junction and causes defects termed cartilaginous (Schmorl's) nodes, within the vertebral body. These nodes exist when a portion of the disk enters a vertebral body. This protrusion can occur only when the cartilaginous endplates has been disrupted*. In this sense, SNd is *pseudo*-SN. However, though SN was initially described based on macroscopic pathology, later

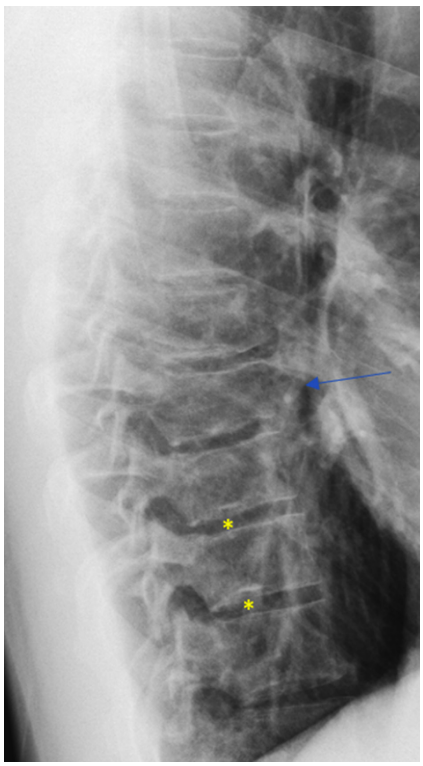

Figure 10 The lower endplates of T9 and T10 both have a small SN with typical location (asterisks, type-1A). T8 has a reduced height (developmental short vertebra), the border of T8 appears to be irregular (arrow). This patient was a 28-year-old man without any symptoms related to spine disorder. Reused with permission from Wáng (16). SN, Schmorl's node.

SN have been primarily diagnosed by *in vivo* imaging. In the past, the vast literature of *in vivo* imaging studies has not differentiated SNd from SNa (8,9,11,14,15,26). For example, in a female twin volunteer study, for their study subjects, Williams *et al.* (26) noted that SNs were more prevalent in the lower endplate than in the upper endplate. The SNs in the example image shown in the paper look like SN type-1A. *Ex vivo* skeletal studies have also included SNd in the broad category of SN (27,28). Therefore, we continue to use the term SN for SNd.

It is highly likely that physical activities can facilitate or exaggerate SNd formation. Sward *et al.* (29) compared vertebral abnormalities in elite gymnasts (males) versus non-athletes (males), they found SNs in 17 out of 24 (71%) gymnasts with nodes in 57 endplates and in 7 out of 16 (44%) non-athletes with nodes in 23 endplates. Sward *et al.* presented spine MR images of 5 cases of gymnasts; it appears all these 5 cases demonstrated features of SN type-1A in its location. In an animal experiment study, Revel *et al.* (30) conducted a histologic study of vertebral end plates on young rats' tails subjected to intensive passive motion. They reported that repetitive mechanical stress on the vertebral body induced the formation of invagination of the nucleus pulposus and cartilage plate through a vertebral end plate disruption. They described that findings were similar to histologic changes observed in Scheuermann's disease.

We have recently analysed 297 cases of Italian Caucasian women, the prevalence of radiographic SN type-1A was 7.4% (22/297) (31). This prevalence is high; however, this study counted all small SNds as well as long as they were visible on spine radiograph. In the same study, for the 297 cases of paired Chinese women, the prevalence of radiographic SNd was only 0.67% (2/297), thus showing marked ethnic difference (31). The vertebral level distribution for SN type-1A among Italian women is shown in *Figure 25*, with the highest prevalence at thoracolumbar junction which is the site with the greatest biomechanical stress. Thus, the vertebral level distribution of SNd is similar to those of high energy vertebral endplate fracture (32) and osteoporotic vertebral endplate fracture (33). In this radiographic study on SN type-1A (31), 16 cases (16/22, 72.7%) had more than one vertebra involvement, while only 6 cases (6/22, 27.3%) had only one vertebra involvement. For vertebrae with SN type-1A, 52.8% had lower endplate involvement, 27.8% had upper endplate involvement, while 19.4% had involved both upper and lower endplates. In a CT chest study, Que *et al.* (2) reported a higher SNd prevalence among Chinese men than among Chinese women. Spine developmental deformities are known to be more common in men than in women. For example, Beutler *et al.* (34) studied 500 children, and 30 subjects with identified pars lesions consisting of 10 women and 20 men. We have recently reviewed lateral chest radiographs of 408 women and 374 men, all with indications other than spine disorders or metabolic disorders. Congenital vertebral deformities were observed in four cases, including one woman and three men (35). We expect SN type-1A prevalence among Caucasian men will be higher.

SN type-1B refers to definite SNd other than that of SN type-1A. The common examples are shown in *Figures 11-16*. Anterior disk herniation may produce a "limbus" vertebra in which the displaced disc tissue separates small bony fragments along the edge of the vertebral body. This results as the disc tissue penetrates vertebral trabeculae at the junction of the cartilaginous and ring apophysis

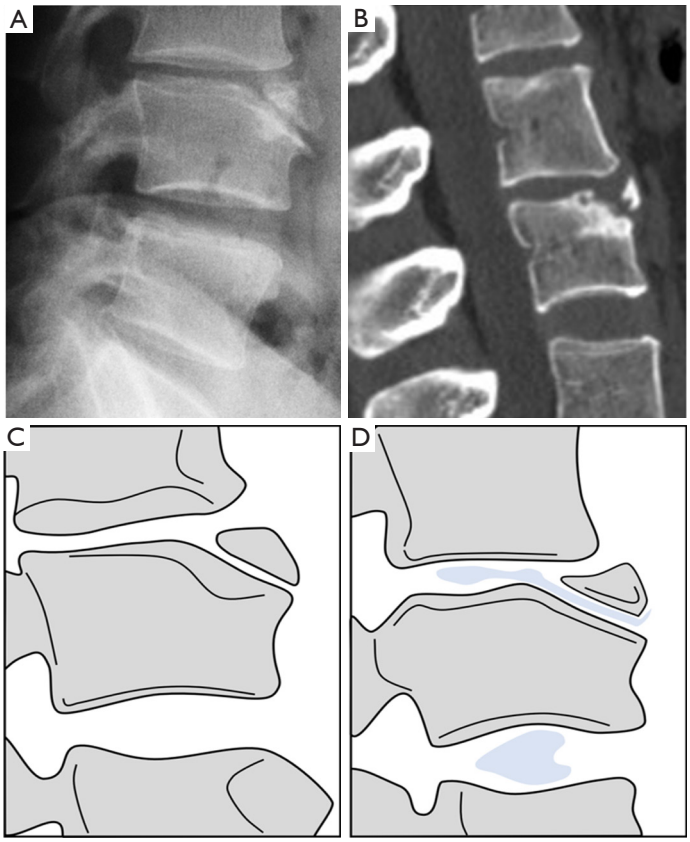

Figure 11 Limbus vertebra with SN type-1B. Radiograph (A) and sagittal reconstruction CT (B) show limbus vertebra. (C) and (D) are line-drawings mimicking the radiograph and radiographic discogram from Ghelman and Freiberger *et al.* (17). Limbus vertebra at L3 level. (D) Mimics discogram of L2–L3 disc showing opacified nucleus pulposus herniated between L2 vertebra body and fragments of limbus vertebra. Discogram at L3–L4 is normal. SN, Schmorl's node; CT, computed tomography.

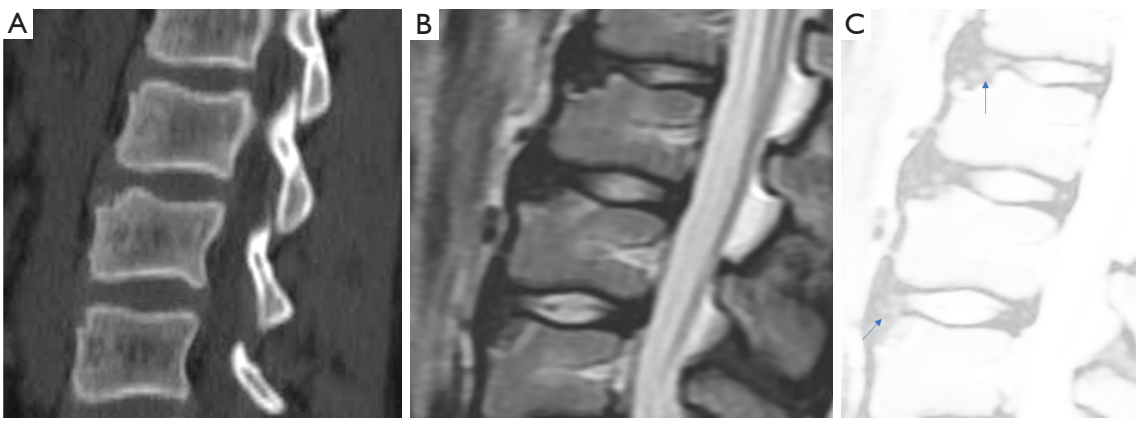

Figure 12 A case has multiple SNs (type-1B). Sagittal reconstructed CT image (A) and T2-weighted MR image (B,C). (C) T2-weighted MR image with heightened brightness tentatively shows disc herniation into the space (arrows). This case has the etiology as illustrated in *Figure 11*. Modified and reused with permission from Wáng *et al.* (18). SN, Schmorl's node; CT, computed tomography; MR, magnetic resonance.

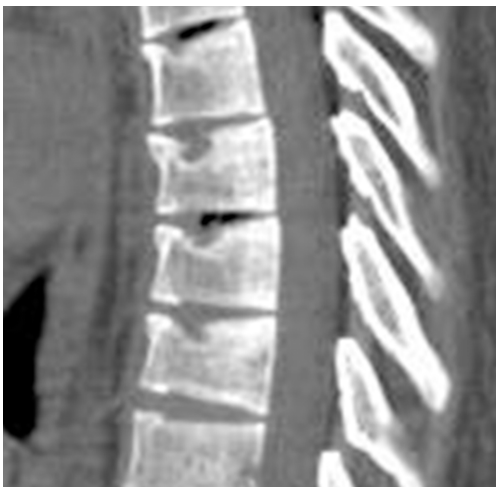

Figure 13 Sagittal reconstructed CT image of thoracic spine shows multiple SNds and mild wedging of vertebral bodies. Multiple nodules with similar locations strongly suggest this case had SNd (type-1B). Overall, these SNd have a clear and continuous sclerotic bony border. Reused with permission from Wáng *et al.* (18). CT, computed tomography; SNd, Schmorl's node of developmental cause.

(17-21,36). Ghelman and Freiberger (17) reported a case where radiographic discogram showed X-ray contrast agent opacified nucleus pulposus herniated between the vertebra body and fragments of limbus vertebra. SNd can co-exist with other spine deformities (*Figure 10*). SNd are known to be a common but not obligate manifestation of Scheuermann disease (*Figures 14,15*).

For SNa, trauma and endplate micro-fractures are known triggers. In a cohort of children who had suffered from stable compressive vertebral fractures, Möller *et al.* (37) reported the occurrence of SN at advanced ages (mean: 40 years; range, 33–53 years) at adjacent disc levels. In a study of 70 thoracolumbar spines from cadavers of individuals killed in motor vehicle collisions, Fahey *et al.* (38) reported a link between trauma and the occurrence of SN. The possible endplate weakness can be due notochord regression, ossification gaps, or vascular channels (20,39), which can facilitate herniation induced by axial forces. However, among older populations, we expect the most common etiology is low bone mineral density (BMD). Recently we described a study of thoracic spine MR imaging

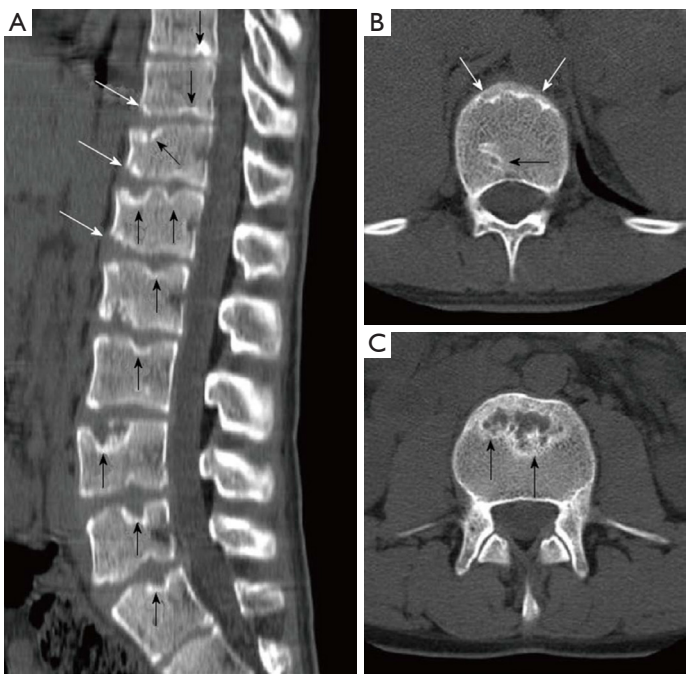

Figure 14 A case of atypical Scheuermann's disease with sagittally reconstructed reformatted (A) and axial CT (B,C). (A) Evident irregularities and SN in thoracic, lumbar, and sacral endplate surfaces (black arrows), anterior wedging in vertebra body (white arrows) are shown; (B,C) endplate irregularities in axial plane CT images (white arrows) and SN (black arrows) are shown. Note that it is not necessary that every single one of these SN is due to Scheuermann's disease. Reused with permission from Gokce and Beyhan (19). CT, computed tomography; SN, Schmorl's node.

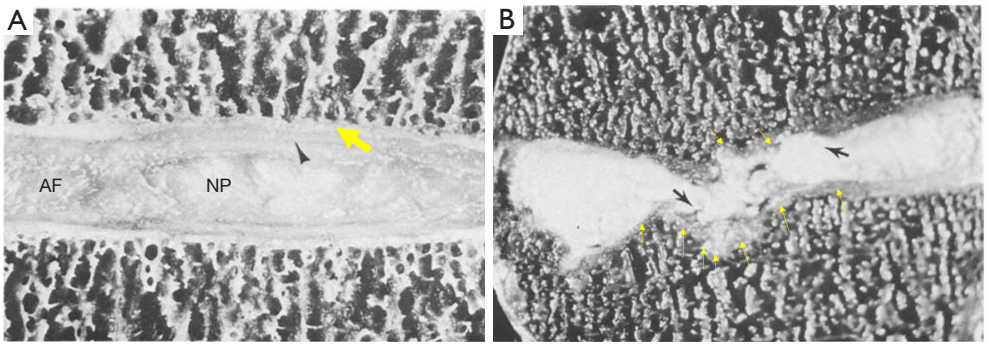

Figure 15 Anatomical image of a normal disc (A) and a disc with Scheuermann's disease (B). Black arrowhead in (A): AF. Yellow thick arrow in (A): cartilaginous endplate. (B) Show multiple Schmorl nodes (black arrows) on both the superior and inferior surface of the vertebral body, where the cartilaginous endplate (yellow arrows) is still continuous. Disk space loss is also seen in (B). Reused with permission from Resnick and Niwayama *et al.* (20). AF, annulus fibrosus; NP, nucleus pulposus.

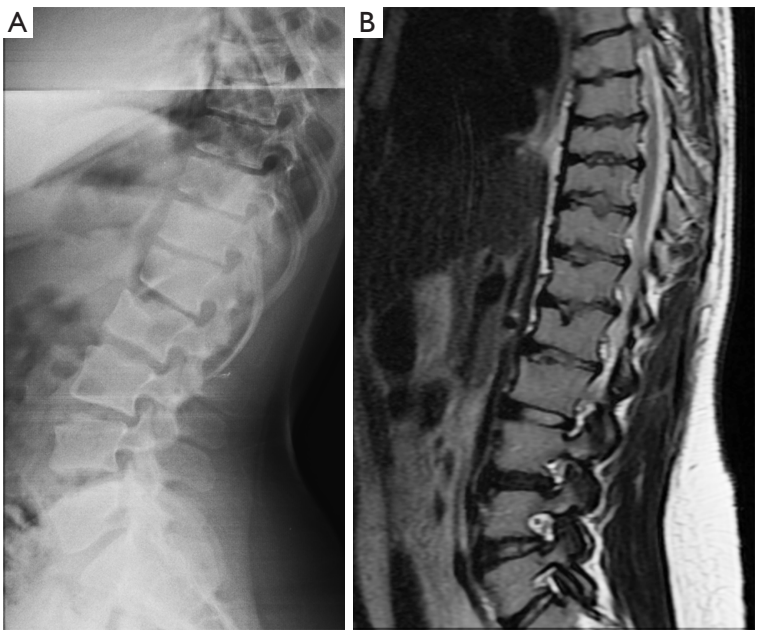

Figure 16 A patient with mucopolysaccharidosis type-1. Lateral spine radiograph (A) and sagittal T2-weighted MRI (B) show multiple hypoplastic vertebral bodies at the thoracolumbar transition, together with multiple SNs (type-1B). These are typical imaging findings of mucopolysaccharidosis. Reused with permission from Wáng *et al.* (18). MRI, magnetic resonance imaging; SN, Schmorl's node.

among community elderly subjects (mean age: 82 years) and noted a number of features of SN paralleled those of osteoporotic-like vertebral fracture (OLVF) (22). SN prevalence in women (55.5%) almost doubled that in men (25.9%). SN was statistically significantly correlated with lower BMD, and subjects with SN were more likely to have OLVF. We did not separate SNa from SNd in that study, but likely the majority of the described SN would have been SNa, as radiographic SNd prevalence is likely low among the Chinese population (31). In vertebrae with osteoporosis, the endplate becomes weakened due to the loss of support from trabecular bone and due to thinning of the endplate itself (40). The vertebral level distribution of SNa will also be similar to traumatic endplate vertebral fracture (high energy trauma) or osteoporotic endplate vertebral fracture (low energy trauma) (22,32,33). The upper endplate is

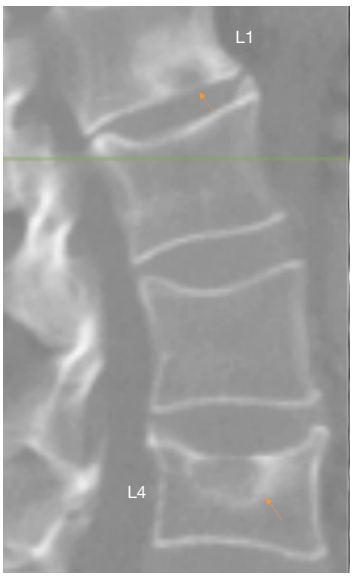

Figure 17 CT image examples of SN type-2 at L4 and at L1. L1 lower endplate SN (arrow: SNa) with apparent reactive bone changes, and L4 with upper endplate SNa (arrow) and depression. SNa at L4 is likely associated with low BMD. Reused with permission from Wáng *et al.* (22). CT, computed tomography; SN, Schmorl's node; SNa, Schmorl's node of acquired cause; BMD, bone mineral density.

less resistant to compressive pressure and more likely to fracture (41). Among elderly subjects, SNa more likely involve upper endplate which is the same as osteoporotic endplate fracture (42), and SNa are commonly associated with endplate depression (1). The herniation of portion of disc materials through endplate into the vertebral spongy bone elicit reactive inflammation. The surrounding sclerosis in vertebra reflects reactive healing response. These reactive bone healing, appearing as a hazy cloud around the SN seen on radiograph or CT, supports the diagnosis of SNa. SNa associated with low BMD are more likely to be modest or large in size, and their borders are not clearly defined on radiograph (*Figures 17-19*).

SNa is better considered as a 'general phenomenon' rather than a specific disease entity where a portion of disc materials herniates through endplate into the vertebral spongy bone (1). In addition to SNa associated with low BMD (22) and SNa associated with acute high energy trauma (24,25,38,43), various other etiology with weakening of the endplate, including infectious spondylodiscitis or other inflammatory spine diseases such as ankylosing spondylitis, may also cause SNa (23,44) (*Figure 23*). Tumorous changes of a vertebra can also increase the fragility of an endplate, and lead to disc materials herniation

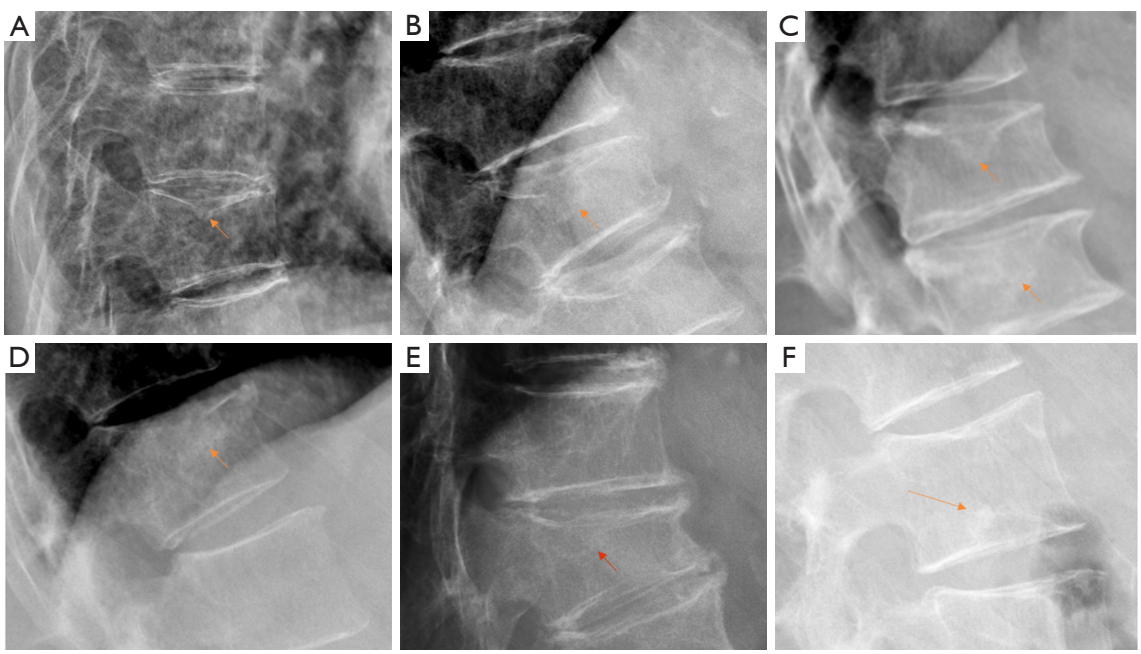

Figure 18 Radiograph shows SNa (type-2, A-F). Overall, these SN have surrounding hazy increased density reflecting reactive bony regeneration (arrow), and the bony sclerotic border may be incomplete. These SNs are not at the most typical location of SNd, and SNa in (A-E) also are associated with osteoporotic-like vertebral fractures. SNa, Schmorl's node of acquired cause; SN, Schmorl's node; SNd, Schmorl's node of developmental cause.

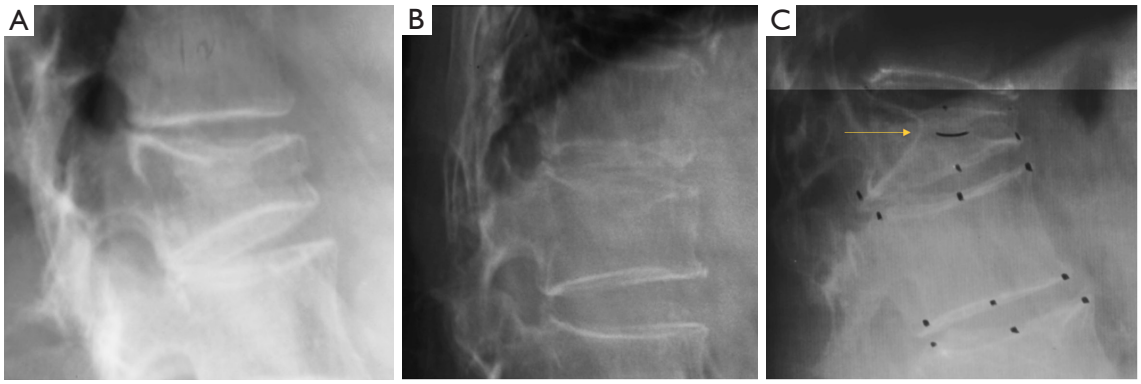

Figure 19 Radiograph of SN (type-2). The bony sclerotic border of these SN is incomplete. Endplate depression is seen in (A) and (B), with hazy increased density surrounding SN reflecting reactive bony regeneration. (C) shows a case of penetrating Schmorl node (arrow), and the involved vertebral body is collapsed due to osteoporosis. SN, Schmorl's node.

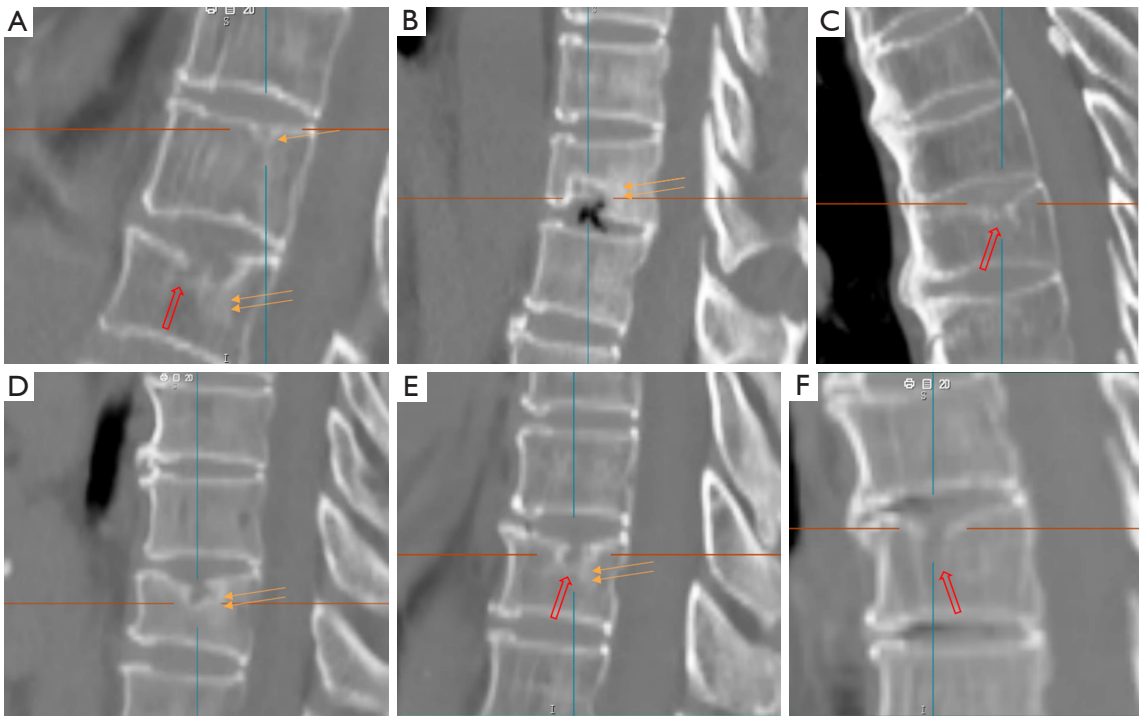

Figure 20 Sagittally reconstructed image show SNa and SNd (A-F). A single arrow denoted an SNd (type-1A) while double arrows and a red open arrow show an SNa (type-2). Double arrows in (A-F) show surrounding hazy increased density reflecting reactive bony regeneration. Red open arrow shows the bony sclerotic border of the SNa is incomplete. SNa, Schmorl's node of acquired cause; SNd, Schmorl's node of developmental cause.

through endplate into the vertebral spongy bone and form SNa (45,46). Peng *et al.* (47) reported that SNa can be the end result of ischaemic necrosis beneath the cartilaginous endplate.

The classification of SNd and SNa has clinical relevance. One important aspect of this classification is that, many of the uncomplicated SNds are developmental imperfection, which may be a weak point for further injury, but they

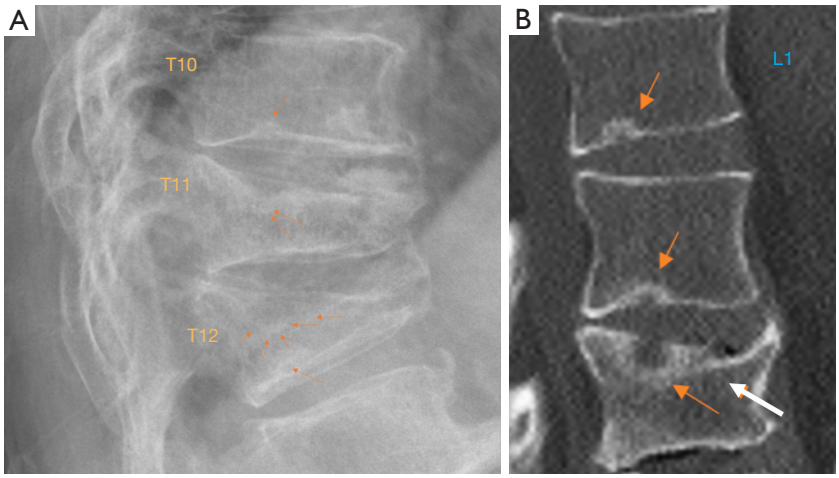

Figure 21 SN of type-1A and type-3, type-4. (A) Radiograph of SN type-1A at T10 and T12 lower endplate (single arrow), and T11 and T12 upper endplate SN type-3. T11 SN shows apparent reactive bone changes around the SN (arrows). T12 upper endplate SN shows an incomplete sclerotic border (arrows). T11 and T12 vertebrae are with collapsed grade osteoporotic fracture. The location of these two upper endplate SN of T11 and T12 is typical of developmental SN (type-1A). (B) Sagittally reconstructed CT image. L1 lower endplate SN type-1A (brown arrow). L2 lower endplate SN type-4. L3 upper endplate SN type-3 (brown arrow), and L3 upper endplate depression (white arrow). SN, Schmorl's node; CT, computed tomography.

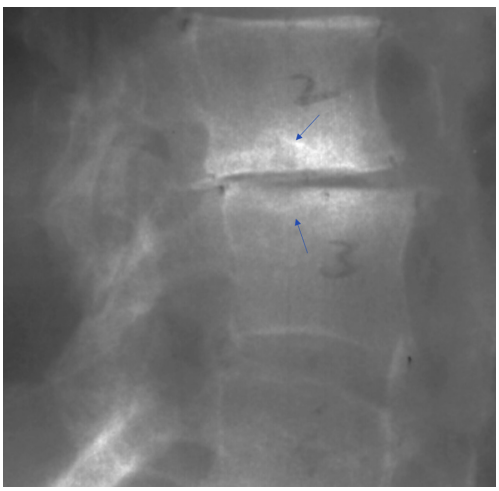

Figure 22 Radiograph of SN type-3 at L2 lower endplate and L3 upper endplate. Arrow shows apparent reactive bone changes while without endplate depression. The location of these two SN is typical of SNd, but the apparent reactive bone changes suggest involvement of acquired cause. There is also intervertebral disc space narrowing. SN, Schmorl's node; SNd, Schmorl's node of developmental cause.

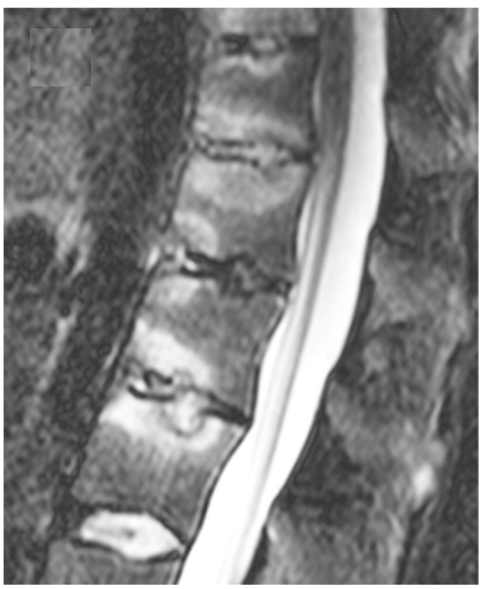

Figure 23 Spinal involvement in axial spondyloarthropathy. STIR images show SN type-3 and inflammatory changes. Reused with permission from Ruiz Santiago *et al.* (23). STIR, sagittal short tau inversion recovery; SN, Schmorl's node.

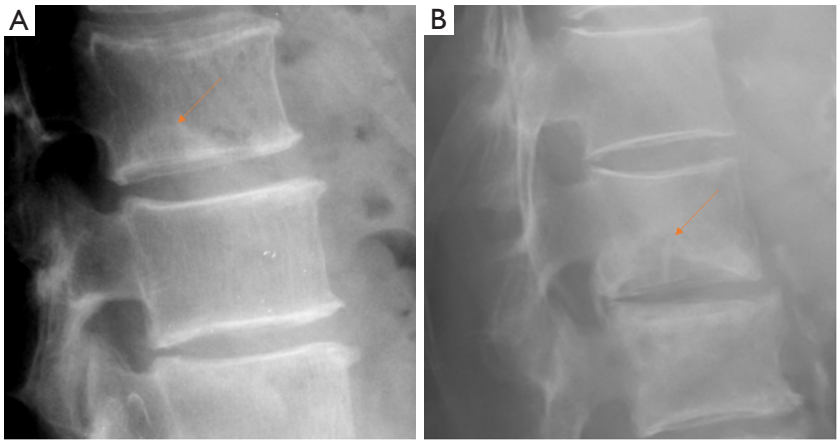

Figure 24 Radiograph of SN type-4 (arrow). Lower endplate SN with possible surrounding reactive bone changes, without endplate depression in (A) and with endplate depression in (B). Bony borders of these two SN are ill-defined. On the other hand, the location of these two SN is typical of SN type-1A. These two SN can be due to pure acquired cause, or due to a mixture of acquired and developmental causes. Particularly for the case in (B), the clinical relevance of this SN will be the same as SN type-2. SN, Schmorl's node.

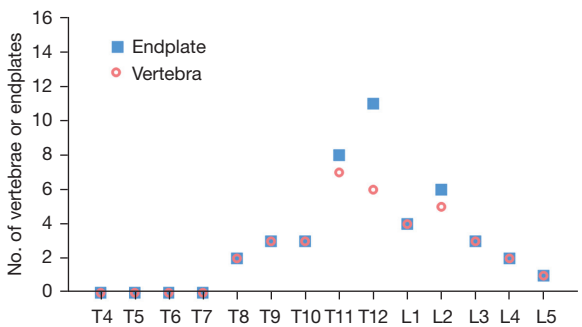

Figure 25 Vertebral level distribution of radiographic SNd (type-1A). X-axis: vertebral level. Y-axis: number of involved vertebra or endplate. Data from 297 cases of Italian Caucasian women with an SNd prevalence of 7.4% (22/297). The highest prevalence is at the thoracolumbar junction which is the site with the greatest biomechanical stress. For vertebrae with SNd (type-1A), 52.8% had lower endplate involvement, 27.8% had upper endplate involvement, while 19.4% had involved both upper and lower endplates. The data in this graph is from Wáng *et al.* (31). SNd, Schmorl's node of developmental cause.

themself do not have a direct clinical consequence. It is also possible that SN type-1A and 'cupid bow' may belong to the same spectrum of developmental changes (1). On the other hand, SNa are associated with cartilaginous endplate disruption, and some SNa may also be an indicator of compromised vertebral bone strength such as osteoporosis (22). Trauma induced SNa may, or may not, heal. We can postulate that SNa during younger age associated higher energy trauma may eventually heal in physiological sense though the morphological deformity may persist. The majority of SNa among older populations is likely due to osteopenia/osteoporosis and these SNa can be progressive. The herniation of disc materials through endplate into the vertebral spongy bone elicits reactive inflammation, which can be sometimes detected by high signal on T2 weighted MR image and increased activity on radioisotope imaging (12,24,25,48,49). Intervertebral discs are the largest avascular structure in the body and can be recognized as foreign matter when met by a well-vascularized source, such as a vertebral body marrow. Such an event may lead to an immune reaction, edema, elevated interosseous pressure, and pain (12,50,51).

Acknowledgments

Funding: None.

Footnote

Conflicts of Interest: The author has completed the ICMJE uniform disclosure form (available at https://qims.amegroups.com/article/view/10.21037/qims-24-335/coif). Y.X.J.W. serves as the Editor-in-Chief of *Quantitative Imaging in Medicine and Surgery*. The author has no other

conflicts of interest to declare.

Ethical Statement: The author is accountable for all aspects of the work in ensuring that questions related to the accuracy or integrity of any part of the work are appropriately investigated and resolved.

References

1. Wáng YXJ. Schmorl's node of primarily developmental cause and Schmorl's node of primarily acquired cause: two related yet different entities. Quant Imaging Med Surg 2023;13:4044-9.
2. Que Y, Zhang M, Luo X, Xia X, Huang Y, Wang C, Chen M, Xu J. Epidemiology of Schmorl's Node in the Thoracic Spine: A Subtype Analysis. Spine (Phila Pa 1976) 2024. [Epub ahead of print]. doi: 10.1097/BRS.0000000000004953.
3. Tsuchiya K, Gomyo M, Katase S, Hiraoka S, Tateishi H. Magnetic resonance bone imaging: applications to vertebral lesions. Jpn J Radiol 2023;41:1173-85.
4. Bae WC, Biswas R, Chen K, Chang EY, Chung CB. UTE MRI of the Osteochondral Junction. Curr Radiol Rep 2014;2:35.
5. Kronthaler S, Boehm C, Feuerriegel G, Börnert P, Katscher U, Weiss K, Makowski MR, Schwaiger BJ, Gersing AS, Karampinos DC. Assessment of vertebral fractures and edema of the thoracolumbar spine based on water-fat and susceptibility-weighted images derived from a single ultra-short echo time scan. Magn Reson Med 2022;87:1771-83.
6. Wei Z, Lombardi AF, Lee RR, Wallace M, Masuda K, Chang EY, Du J, Bydder GM, Yang W, Ma YJ. Comprehensive assessment of in vivo lumbar spine intervertebral discs using a 3D adiabatic T1ρ prepared ultrashort echo time (UTE-Adiab-T1ρ) pulse sequence. Quant Imaging Med Surg 2022;12:269-80.
7. Ma Y, Jang H, Jerban S, Chang EY, Chung CB, Bydder GM, Du J. Making the invisible visible-ultrashort echo time magnetic resonance imaging: Technical developments and applications. Appl Phys Rev 2022;9:041303.
8. Siriwanarangsun P, Statum S, Biswas R, Bae WC, Chung CB. Ultrashort time to echo magnetic resonance techniques for the musculoskeletal system. Quant Imaging Med Surg 2016;6:731-43.
9. Lombardi AF, Wei Z, Wong J, Carl M, Lee RR, Wallace M, Masuda K, Chang EY, Du J, Ma YJ. High contrast cartilaginous endplate imaging using a 3D adiabatic inversion-recovery-prepared fat-saturated ultrashort echo time (3D IR-FS-UTE) sequence. NMR Biomed 2021;34:e4579.
10. Athertya JS, Lo J, Chen X, Shin SH, Malhi BS, Jerban S, Ji Y, Sedaghat S, Yoshioka H, Du J, Guma M, Chang EY, Ma Y. High contrast cartilaginous endplate imaging in spine using three dimensional dual-inversion recovery prepared ultrashort echo time (3D DIR-UTE) sequence. Skeletal Radiol 2024;53:881-90.
11. Chen KC, Tran B, Biswas R, Statum S, Masuda K, Chung CB, Bae WC. Evaluation of the disco-vertebral junction using ultrashort time-to-echo magnetic resonance imaging: inter-reader agreement and association with vertebral endplate lesions. Skeletal Radiol 2016;45:1249-56.
12. Lotz JC, Fields AJ, Liebenberg EC. The role of the vertebral end plate in low back pain. Global Spine J 2013;3:153-64.
13. Law T, Anthony MP, Chan Q, Samartzis D, Kim M, Cheung KM, Khong PL. Ultrashort time-to-echo MRI of the cartilaginous endplate: technique and association with intervertebral disc degeneration. J Med Imaging Radiat Oncol 2013;57:427-34.
14. Finkenstaedt T, Siriwananrangsun P, Masuda K, Bydder GM, Chen KC, Bae WC. Ultrashort time-to-echo MR morphology of cartilaginous endplate correlates with disc degeneration in the lumbar spine. Eur Spine J 2023;32:2358-67.
15. Ji Z, Li Y, Dou W, Zhu Y, Shi Y, Zou Y. Ultra-short echo time MR imaging in assessing cartilage endplate damage and relationship between its lesion and disc degeneration for chronic low back pain patients. BMC Med Imaging 2023;23:60.
16. Wáng YXJ. A summary of our recent evidence-based works on radiographic diagnostics of prevalent osteoporotic vertebral fracture in older men and women. Quant Imaging Med Surg 2023;13:1264-85.
17. Ghelman B, Freiberger RH. The limbus vertebra: an anterior disc herniation demonstrated by discography. AJR

Am J Roentgenol 1976;127:854-5.
18. Wáng YXJ, Santiago FR, Deng M, Nogueira-Barbosa MH. Identifying osteoporotic vertebral endplate and cortex fractures. Quant Imaging Med Surg 2017;7:555-91.
19. Gokce E, Beyhan M. Radiological imaging findings of scheuermann disease. World J Radiol 2016;8:895-901.
20. Resnick D, Niwayama G. Intravertebral disk herniations: cartilaginous (Schmorl's) nodes. Radiology 1978;126:57-65.
21. Dietemann JL, Runge M, Badoz A, Dosch JC, Beaujeux R, Bonneville JF, Wackenheim A. Radiology of posterior lumbar apophyseal ring fractures: report of 13 cases. Neuroradiology 1988;30:337-44.
22. Wáng YXJ, Wang XR, Leung JCS, Yu BWM, Griffith JF, Kwok TCY. Schmorl's nodes are associated with prevalent osteoporotic vertebral fracture and low bone mineral density: a population-based thoracic spine MRI study in older men and women. Quant Imaging Med Surg 2023;13:1914-26.
23. Ruiz Santiago F, Láinez Ramos-Bossini AJ, Wáng YXJ, Martínez Barbero JP, García Espinosa J, Martínez Martínez A. The value of magnetic resonance imaging and computed tomography in the study of spinal disorders. Quant Imaging Med Surg 2022;12:3947-86.
24. Seymour R, Williams LA, Rees JI, Lyons K, Lloyd DC. Magnetic resonance imaging of acute intraosseous disc herniation. Clin Radiol 1998;53:363-8.
25. Walters G, Coumas JM, Akins CM, Ragland RL. Magnetic resonance imaging of acute symptomatic Schmorl's node formation. Pediatr Emerg Care 1991;7:294-6.
26. Williams FM, Manek NJ, Sambrook PN, Spector TD, Macgregor AJ. Schmorl's nodes: common, highly heritable, and related to lumbar disc disease. Arthritis Rheum 2007;57:855-60.
27. Saluja G, Fitzpatrick K, Bruce M, Cross J. Schmorl's nodes (intravertebral herniations of intervertebral disc tissue) in two historic British populations. J Anat 1986;145:87-96.
28. Pfirrmann CW, Resnick D. Schmorl nodes of the thoracic and lumbar spine: radiographic-pathologic study of prevalence, characterization, and correlation with degenerative changes of 1,650 spinal levels in 100 cadavers. Radiology 2001;219:368-74.
29. Swärd L, Hellström M, Jacobsson B, Nyman R, Peterson L. Disc degeneration and associated abnormalities of the spine in elite gymnasts. A magnetic resonance imaging study. Spine (Phila Pa 1976) 1991;16:437-43.
30. Revel M, Andre-Deshays C, Roudier R, Roudier B, Hamard G, Amor B. Effects of repetitive strains on vertebral end plates in young rats. Clin Orthop Relat Res 1992;(279):303-9.
31. Wáng YXJ, Diacinti D, Iannacone A, Kripa E, Leung JCS, Kwok TCY, Diacinti D. A comparison of radiographic degeneration features of older Chinese women and older Italian Caucasian women with a focus on thoracic spine. Aging Clin Exp Res 2023;35:2583-91.
32. Wang XR, Xu FR, Huang QL, Wáng YXJ. Radiological features of traumatic vertebral endplate fracture: an analysis of 194 cases with 263 vertebral fractures. Chin Med J (Engl) 2020;133:2696-702.
33. Wáng YXJ, Diacinti D, Leung JCS, Iannacone A, Kripa E, Kwok TCY, Diacinti D. Much lower prevalence and severity of radiographic osteoporotic vertebral fracture in elderly Hong Kong Chinese women than in age-matched Rome Caucasian women: a cross-sectional study. Arch Osteoporos 2021;16:174.
34. Beutler WJ, Fredrickson BE, Murtland A, Sweeney CA, Grant WD, Baker D. The natural history of spondylolysis and spondylolisthesis: 45-year follow-up evaluation. Spine (Phila Pa 1976) 2003;28:1027-35; discussion 1035.
35. Ma JB, Wáng YXJ. Chest radiograph prevalence of vertebral deformity among young and middle-aged population of mixed city dwellers and rural residents. J Thorac Dis 2022;14:4685-98.
36. Henales V, Hervás JA, López P, Martínez JM, Ramos R, Herrera M. Intervertebral disc herniations (limbus vertebrae) in pediatric patients: report of 15 cases. Pediatr Radiol 1993;23:608-10.
37. Möller A, Maly P, Besjakov J, Hasserius R, Ohlin A, Karlsson MK. A vertebral fracture in childhood is not a risk factor for disc degeneration but for Schmorl's nodes: a mean 40-year observational study. Spine (Phila Pa 1976) 2007;32:2487-92.
38. Fahey V, Opeskin K, Silberstein M, Anderson R, Briggs C. The pathogenesis of Schmorl's nodes in relation to acute trauma. An autopsy study. Spine (Phila Pa 1976) 1998;23:2272-5.
39. Chandraraj S, Briggs CA, Opeskin K. Disc herniations in the young and end-plate vascularity. Clin Anat 1998;11:171-6.
40. Wang YX, Griffith JF. Menopause causes vertebral endplate degeneration and decrease in nutrient diffusion to the intervertebral discs. Med Hypotheses 2011;77:18-20.
41. Zhao FD, Pollintine P, Hole BD, Adams MA, Dolan P. Vertebral fractures usually affect the cranial endplate because it is thinner and supported by less-dense trabecular bone. Bone 2009;44:372-9.
42. Che-Nordin N, Deng M, Griffith JF, Leung JCS, Kwok

AWL, Zhu YQ, So RHY, Kwok TCY, Leung PC, Wáng YXJ. Prevalent osteoporotic vertebral fractures more likely involve the upper endplate than the lower endplate and even more so in males. Ann Transl Med 2018;6:442.
43. Lundin O, Ekström L, Hellström M, Holm S, Swärd L. Exposure of the porcine spine to mechanical compression: differences in injury pattern between adolescents and adults. Eur Spine J 2000;9:466-71.
44. Cawley MI, Chalmers TM, Kellgren JH, Ball J. Destructive lesions of vertebral bodies in ankylosing spondylitis. Ann Rheum Dis 1972;31:345-58.
45. Grivé E, Rovira A, Capellades J, Rivas A, Pedraza S. Radiologic findings in two cases of acute Schmörl's nodes. AJNR Am J Neuroradiol 1999;20:1717-21.
46. Yamaguchi T, Suzuki S, Ishiiwa H, Yamato M, Ueda Y. Schmorl's node developing in the lumbar vertebra affected with metastatic carcinoma: correlation magnetic resonance imaging with histological findings. Spine (Phila Pa 1976) 2003;28:E503-5.
47. Peng B, Wu W, Hou S, Shang W, Wang X, Yang Y. The pathogenesis of Schmorl's nodes. J Bone Joint Surg Br 2003;85:879-82.
48. Takahashi K, Miyazaki T, Ohnari H, Takino T, Tomita K. Schmorl's nodes and low-back pain. Analysis of magnetic resonance imaging findings in symptomatic and asymptomatic individuals. Eur Spine J 1995;4:56-9.
49. Wáng YXJ, Wu AM, Ruiz Santiago F, Nogueira-Barbosa MH. Informed appropriate imaging for low back pain management: A narrative review. J Orthop Translat 2018;15:21-34.
50. Zhang N, Li FC, Huang YJ, Teng C, Chen WS. Possible key role of immune system in Schmorl's nodes. Med Hypotheses 2010;74:552-4.
51. Abel F, Altorfer FCS, Rohatgi V, Gibbs W, Chazen JL. Imaging of Discogenic and Vertebrogenic Pain. Radiol Clin North Am 2024;62:217-28.

Cite this article as: Wáng YXJ. Cartilaginous endplate coverage of developmental Schmorl's node and the relevance of this in Schmorl's node etiology-based classification. Quant Imaging Med Surg 2024;14(6):4288-4303. doi: 10.21037/qims-24-335

